REPORT DOCUMENTATION PAGE

Form Approved
OMB No. 0704-0188

1. REPORT DATE *(DD-MM-YYYY)*	2. REPORT TYPE	3. DATES COVERED *(From - To)*
10-11-2004	REPRINT	

4. TITLE AND SUBTITLE
Low-altitude distribution of radiation belt electrons

5a. CONTRACT NUMBER

5b. GRANT NUMBER

5c. PROGRAM ELEMENT NUMBER
62601F

6. AUTHOR(S)
R. S. Selesnick*, M. D. Looper* and
Jay M. Albert

5d. PROJECT NUMBER
1010

5e. TASK NUMBER
RS

5f. WORK UNIT NUMBER
A1

7. PERFORMING ORGANIZATION NAME(S) AND ADDRESS(ES)
Air Force Research Laboratory/VSBX
29 Randolph Road
Hanscom AFB, MA 01731-3010

8. PERFORMING ORGANIZATION REPORT NUMBER
AFRL-VS-HA-TR-2004-1205

9. SPONSORING/MONITORING AGENCY NAME(S) AND ADDRESS(ES)

10. SPONSOR/MONITOR'S ACRONYM(S)

11. SPONSOR/MONITOR'S REPORT NUMBER(S)

12. DISTRIBUTION/AVAILABILITY STATEMENT
Approved for public release; distribution unlimited

13. SUPPLEMENTARY NOTES
REPRINTED FROM: J. Geophysical Res., Vol. 109, A11209, doi:10.1029/2004JA010611, 2004. *Aerospace Corporation, Los Angeles, CA

14. ABSTRACT
A numerical simulation of the low-altitude electron radiation belt is described. It includes dependences on the electron's bounce and drift phases, equatorial pitch angle, and kinetic energy in the range of ~1 to several MeV at L = 3.5. Physical processes in addition to the adiabatic electron motion are pitch angle diffusion and backscattering from a realistic model atmosphere. Quasi-linear diffusion coefficients are calculated from a model of the whistler mode plasmaspheric hiss wave intensity. Comparisons of the simulation results with electron data from a low-altitude satellite show that the model accounts for the main features of the electron spatial distribution during selected periods of differing geomagnetic activity.

15. SUBJECT TERMS
Radiation belt Electrons Diffusion Atmospheric scattering

16. SECURITY CLASSIFICATION OF:			17. LIMITATION OF ABSTRACT	18. NUMBER OF PAGES	19a. NAME OF RESPONSIBLE PERSON
a. REPORT	b. ABSTRACT	c. THIS PAGE			Jay M. Albert
UNCL	UNCL	UNCL	UNL		19b. TELEPHONE NUMBER *(Include area code)* (781) 377-3992

JOURNAL OF GEOPHYSICAL RESEARCH, VOL. 109, A11209, doi:10.1029/2004JA010611, 2004

Low-altitude distribution of radiation belt electrons

R. S. Selesnick and M. D. Looper
The Aerospace Corporation, Los Angeles, California, USA

J. M. Albert
Space Vehicles Directorate, Air Force Research Laboratory, Hanscom Air Force Base, Massachusetts, USA

Received 3 June 2004; revised 17 August 2004; accepted 27 August 2004; published 10 November 2004.

[1] A numerical simulation of the low-altitude electron radiation belt is described. It includes dependences on the electrons' bounce and drift phases, equatorial pitch angle, and kinetic energy in the range of ~1 to several MeV at $L = 3.5$. Physical processes in addition to the adiabatic electron motion are pitch angle diffusion and backscattering from a realistic model atmosphere. Quasi-linear diffusion coefficients are calculated from a model of the whistler mode plasmaspheric hiss wave intensity. Comparisons of the simulation results with electron data from a low-altitude satellite show that the model accounts for the main features of the electron spatial distribution during selected periods of differing geomagnetic activity. *INDEX TERMS:* 2720 Magnetospheric Physics: Energetic particles, trapped; 2716 Magnetospheric Physics: Energetic particles, precipitating; 2753 Magnetospheric Physics: Numerical modeling; 2772 Magnetospheric Physics: Plasma waves and instabilities; *KEYWORDS:* radiation belt, electrons, diffusion, atmospheric scattering

Citation: Selesnick, R. S., M. D. Looper, and J. M. Albert (2004), Low-altitude distribution of radiation belt electrons, *J. Geophys. Res.*, *109*, A11209, doi:10.1029/2004JA010611.

1. Introduction

[2] The distribution of radiation belt electrons is considerably more complex at low altitudes than at high altitudes because of the interaction with the atmosphere combined with the non-dipolar nature of the geomagnetic field. Radiation belt populations whose mirror points do not reach the atmosphere can usually be described by an average over all three phases of the adiabatic particle motion: the gyration phase about the local magnetic field direction, the bounce phase along the magnetic field line between the mirror points, and the drift phase around the Earth. This averaging reduces the dimensionality of the phase space density f from 6 to 3. The asymmetric geomagnetic field allows the possibility of mirror points both above and below the top of the atmosphere within the adiabatic motion of a single particle. In a population where a substantial fraction of the mirror points are within or below the dense atmosphere, f is likely to have a strong dependence on the both the bounce and drift phases, so that averaging over those two variables is inadvisable and the dimensionality of f is reduced then only to 5. Satellites in low Earth orbit (with altitudes 10^3 km) encounter such a population of radiation belt electrons. Therefore it is desirable that radiation belt models for application to such orbits should retain both the bounce and drift phase dependencies.

[3] Low-altitude satellites spend a large fraction of their observing time within the bounce loss cone, that region of momentum space for which the mirror points are below the atmosphere in either hemisphere. Numerical modeling of the bounce loss cone electron distribution, including the bounce phase dependence and electron backscattering from the atmosphere, was described by *Davidson and Walt* [1977]. An analytic approximation with asymptotic matching of the trapped electron distribution was described by *Retterer et al.* [1983]. These models were applicable to the auroral electron kinetic energies of ~10 keV, for which the drift timescales are relatively long and the drift phase dependence of the electron distribution can reasonably be neglected.

[4] For electrons with kinetic energies ~1 MeV the azimuthal drift motion is significant. A numerical model of their distribution, including the drift phase dependence and pitch angle diffusion from the stably trapped population into the quasi-trapped population was described by *Selesnick et al.* [2003]. As the geographic longitude of a low-altitude satellite varies, either by its orbital motion or by the rotation of the Earth, it is accessible to a varying fraction of electron trajectories that are either stably trapped, with the drift shell entirely above the dense atmosphere, or quasi-trapped, with mirror points below the dense atmosphere at a remote longitude. The quasi-trapped electrons are outside the local bounce loss cone but are in the drift loss cone because their drift motion will eventually take them into the bounce loss cone. The trapped and quasi-trapped electron intensities are usually significantly higher than those of the untrapped (or bounce loss cone) electrons, so they can be the dominant contributors to the total electron fluence over an orbital timescale.

[5] The energetic ~1 MeV electrons can also include a significant bounce loss cone population. To describe this population it is necessary to combine the two types of calculations described above into a single model that includes both the bounce and drift phase dependences. That

0148-0227/04/2004JA010611$09.00

is the goal of this work. The model has three main inputs: a description of the electron scattering by the atmosphere based on Monte Carlo simulations, the pitch angle diffusion coefficients derived from the theory of wave particle interactions, and the initial stably trapped electron distribution obtained from satellite measurements. By comparing the model results with observations of the bounce and drift loss cone electron distributions we can then determine whether these model elements are sufficient to describe the main spatial variations in those electron populations. Such calculations can also be of practical value for predicting the range of electron intensities in various low Earth orbits.

2. Model Description

2.1. Transport Equation

[6] Stochastic pitch angle scattering at constant energy can be described by a one-dimensional Fokker-Plank equation based on the spherical volume element in momentum space, with only the pitch angle α allowed to vary. With the condition that the steady state solution be isotropic, the friction and diffusion terms can be combined. The resulting diffusion equation is

$$\frac{\partial f}{\partial t} = \frac{1}{\sin\alpha}\frac{\partial}{\partial \alpha}\left(\sin\alpha D_{\alpha\alpha}\frac{\partial f}{\partial \alpha}\right), \tag{1}$$

where t is time and $D_{\alpha\alpha}$ is the diffusion coefficient.

[7] It is useful to account for conservation of the first adiabatic invariant by a change of variables from α to $x = \cos\alpha_0$, where α_0 is the equatorial pitch angle. With additional terms to describe the radiation belt dynamics the result is

$$\frac{\partial f}{\partial t} + v\cos\alpha\frac{\partial f}{\partial s} + \omega_d\frac{\partial f}{\partial \phi} = \frac{\cos\alpha}{x}\frac{\partial}{\partial x}\left(\frac{x}{\cos\alpha}D_{xx}\frac{\partial f}{\partial x}\right) + Q - L, \tag{2}$$

where

$$\cos\alpha = \sqrt{1 - \frac{B}{B_0}(1-x^2)}, \tag{3}$$

v is the constant electron speed, s is the distance along the magnetic field line, ω_d is the azimuthal drift rate, ϕ is the azimuth around the drift shell (or drift phase), $D_{xx} = (\partial\alpha/\partial x)^2 D_{\alpha\alpha}$ is the x diffusion coefficient, Q and L are local source and loss terms respectively, and finally B and B_0 are respectively the local and equatorial magnetic field magnitude. The second and third terms account respectively for the parallel bounce motion [*Davidson and Walt*, 1977] and the azimuthal drift motion [*Selesnick et al.*, 2003]. This transport equation neglects radial diffusion and energy diffusion, which are significant at some times and locations in the radiation belt. The boundary conditions at $x = \pm 1$ are $\partial f/\partial x = 0$ because there than can be no diffusion into or out of the unphysical x region.

[8] The source and loss terms are included in (2) to account for atmospheric scattering and energy degradation:

$$Q = v\cos\alpha\left[\delta(s - s^N_{atm})f^N_{BS} + \delta(s - s^S_{atm})f^S_{BS}\right] \tag{4}$$

$$L = v\cos\alpha\left[\delta(s - s^N_{atm}) + \delta(s - s^S_{atm})\right]f, \tag{5}$$

where $\delta(s)$ is the Dirac delta function. All electrons reaching the location of the dense atmosphere, at $s = s^N_{atm}$ or s^S_{atm} in the northern or southern hemisphere respectively, are considered to be lost. The corresponding backscattered distributions at the same locations, f^N_{BS} and f^S_{BS}, which depend on f, are considered to be electron sources. This description is possible if there is a sharp demarcation between the trapping region and the region of rapid atmospheric scattering, that is, the bounce loss cone is well defined, which is true for $L \gtrsim 1.2$ [*Walt*, 1966].

[9] For describing the stably trapped radiation belt population it is usual to introduce bounce and drift averaging. This will also turn out to be useful for our numerical solution of the model equation (2). The bounce average of any quantity u is generally defined by the field line integral

$$\langle u\rangle_b = \frac{1}{\tau_b}\oint\frac{u}{v\cos\alpha}ds \tag{6}$$

taken over a complete bounce cycle, where τ_b is the bounce period (defined with $u = 1$). The bounce averaged transport equation is obtained by assuming that f is independent of s [*Retterer et al.*, 1983]:

$$\frac{\partial f}{\partial t} + \langle\omega_d\rangle_b\frac{\partial f}{\partial \phi} = \frac{1}{\tau_b x}\frac{\partial}{\partial x}\left(\tau_b x\langle D_{xx}\rangle_b\frac{\partial f}{\partial x}\right) + \langle Q - L\rangle_b \tag{7}$$

which, by symmetry about $x = 0$, applies to the interval $0 \le x \le 1$ with $\partial f/\partial x = 0$ at each boundary. The bounce averaged source and loss terms are nonzero only at x values for which either or both mirror points are below the top of the atmosphere:

$$\langle Q - L\rangle_b = \frac{1}{\tau_b}\left[(f^N_{BS} - f)\Theta(x^N_c - x) + (f^S_{BS} - f)\Theta(x^S_c - x)\right], \tag{8}$$

where $\Theta(x)$ is the unit step function ($\Theta = 1$ for $x > 0$, $\Theta = 0$ for $x < 0$). The x values x^N_c and x^S_c correspond to electrons with mirror points at $s = s^N_{atm}$ and s^S_{atm} respectively. These define the north and south bounce loss cones.

[10] In the case of an axisymmetric magnetic field, such as a dipole, it is simple to define the drift average as the average over ϕ. Then the bounce and drift averaged transport equation is

$$\frac{\partial f}{\partial t} = \frac{1}{\tau_b x}\frac{\partial}{\partial x}\left(\tau_b x\langle D_{xx}\rangle_{b,d}\frac{\partial f}{\partial x}\right) + \langle Q - L\rangle_{b,d}, \tag{9}$$

where $\langle u\rangle_{b,d}$ is the bounce and drift average of u. This equation does not strictly apply to non-axisymmetric magnetic fields because τ_b and ω_d would be ϕ dependent, but it is a reasonable approximation for the Earth's inner magnetosphere.

2.2. Atmospheric Backscattering

[11] The north and south backscattered electron distributions at a given energy E are related to the distribution f

entering the atmosphere at energies greater than E, because of energy loss during the scattering process:

$$f_{BS}^{N}(\alpha, E) = \int_{E}^{\infty} \int_{0}^{\frac{\pi}{2}} f(s_{atm}^{N}, \alpha', E') \mathcal{S}(\alpha, E, \alpha', E') \sin \alpha' d\alpha' dE' \tag{10}$$

for $\frac{\pi}{2} \leq \alpha \leq \pi$ and

$$f_{BS}^{S}(\alpha, E) = \int_{E}^{\infty} \int_{\frac{\pi}{2}}^{\pi} f(s_{atm}^{S}, \alpha', E') \mathcal{S}(\pi - \alpha, E, \pi - \alpha', E') \cdot \sin \alpha' d\alpha' dE' \tag{11}$$

for $0 \leq \alpha \leq \frac{\pi}{2}$, where α' and α are local pitch angles at $s = s_{atm}^{N}$ or s_{atm}^{S}, and the scattering function $\mathcal{S}$ is defined for α' values entering the atmosphere and α values leaving the atmosphere in the northern hemisphere.

[12] The scattering function $\mathcal{S}$ is the backscattered electron distribution at the top of the atmosphere from incident electrons of fixed energy and pitch angle that are uniformly distributed in gyrophase. To calculate $\mathcal{S}$ we use the EGSnrc Monte Carlo code for electron and photon transport [*Kawrakow and Rogers*, 2000]. The magnetic field is that of a centered dipole at $L = 3.8$ and 200 km altitude. The incident electrons and the products of the resulting electron-γ ray showers are followed through the atmosphere accounting for their motion in the local magnetic field. Electrons of each sample energy and pitch angle are started at an altitude of 200 km, above the dense atmosphere, and the emerging electron distribution is collected at 205 km altitude (slightly higher than the start to allow for some altitude increase during the initial gyration about the magnetic field). The atmosphere below 200 km is constructed of 1 km thick layers containing atomic and molecular O, N, and Ar in abundances determined by the NRLMSISE-00 model atmosphere [*Picone et al.*, 2002] averaged over geographic and temporal variations.

[13] Sample results from this calculation are shown in Figure 1 for two different incident electron energies E' and pitch angles α'. In each case $\mathcal{S}$ is strongly peaked at energies just below the incident energy, but there is also a significant contribution to the total number of backscattered electrons at energies E well below the incident energy E'. The pitch angles of the backscattered electrons are generally modified significantly from those that would be obtained by mirroring of the incident electrons in the dipole field. The changes in backscattered pitch angle and energy increase as the incident pitch angle takes the electrons deeper into the atmosphere. The total albedo, or fraction of incident electrons that emerge from the atmosphere at any energy or pitch angle, is shown in Figure 2 as a function of incident pitch angle α' for selected values of the incident energy E'. The total albedo is seen to decrease significantly with increasing energy except at the higher pitch angles where the reverse is true. This is because only the lower-energy electrons are strongly scattered in direction, so for incident trajectories with mirror points well below the top of the atmosphere the low energies can easily be scattered back out while the high energies reach deep into the atmosphere before losing enough energy to be scattered. For incident trajectories with mirror points in the high, tenuous atmosphere, the low-energy electrons can be scattered into the deep atmosphere and lost, while the high-energy electrons simply mirror without scattering. The mirror force of the magnetic field in the atmosphere also acts to increase the albedo relative to that with no magnetic field.

2.3. Diffusion Coefficients

[14] Electron pitch angle diffusion by cyclotron resonance with whistler mode waves has been described by *Lyons* [1974] and *Albert* [1999]. The local quasi-linear diffusion coefficient is proportional to the square of the wave magnetic field b_w^2 and is a complex function of a set of wave parameters that describe the distribution of wave power in frequency and propagation direction, and of the local plasma density. At $L = 3.5$, the main contribution to the whistler mode power is from plasmaspheric hiss. Sample diffusion coefficients D_{xx} at $L = 3.5$, calculated by the method of *Albert* [1999], are shown in Figure 3 as a function of x for two different electron energies and for selected magnetic latitudes. They used nominal hiss wave and plasma parameters described by *Albert* [1999], based on those of *Abel and Thorne* [1998a]. For each magnetic latitude, there is a sharp peak at low x that is a result of the Landau ($n = 0$) resonance of electrons near their mirror points (α near 90°). The continua at higher x values are due to the higher-order resonances.

[15] The calculated model diffusion coefficients can be scaled by b_w^2 for different values of the local wave power (Figure 3 used $b_w = 10$ pT). Separate calculations would be required if any of the other wave or plasma parameters were varied, but, because they are not well known, we use just their nominal values. The sensitivity of the diffusion coefficients to the various wave and plasma parameters has been described by *Abel and Thorne* [1998b] and by *Albert* [1999].

[16] The hiss intensity is known to vary with magnetic local time, being generally highest on the day side [*André et al.*, 2002; *Selesnick et al.*, 2003]. Therefore we have chosen to model the square of the wave field b_w^2 as varying sinusoidally in magnetic local time with a maximum at noon and a minimum, that is a factor of 10 lower, at midnight. The intensity is also known to increase with geomagnetic activity [*Smith et al.*, 1974; *André et al.*, 2002]. Therefore, for the noon maxima we have chosen three representative values, $b_w = 31$, 54, and 100 pT, to cover a range of magnetospheric conditions. We assume the wave intensity to be distributed uniformly along the magnetic field lines.

3. Model Solutions

3.1. Numerical Method

[17] For times of steady radiation belt decay the time dependence of f can be separated from the spatial dependence as an exponential with a time constant that determines the e-folding electron lifetime. In our numerical solution, the finite difference approximation to the transport equation is integrated forward in time from an initial condition until the steady decay is reached. Then the lifetimes can be obtained directly from the decay rate of the numerical solution or from an s, x, and ϕ average of $L - Q$, the net

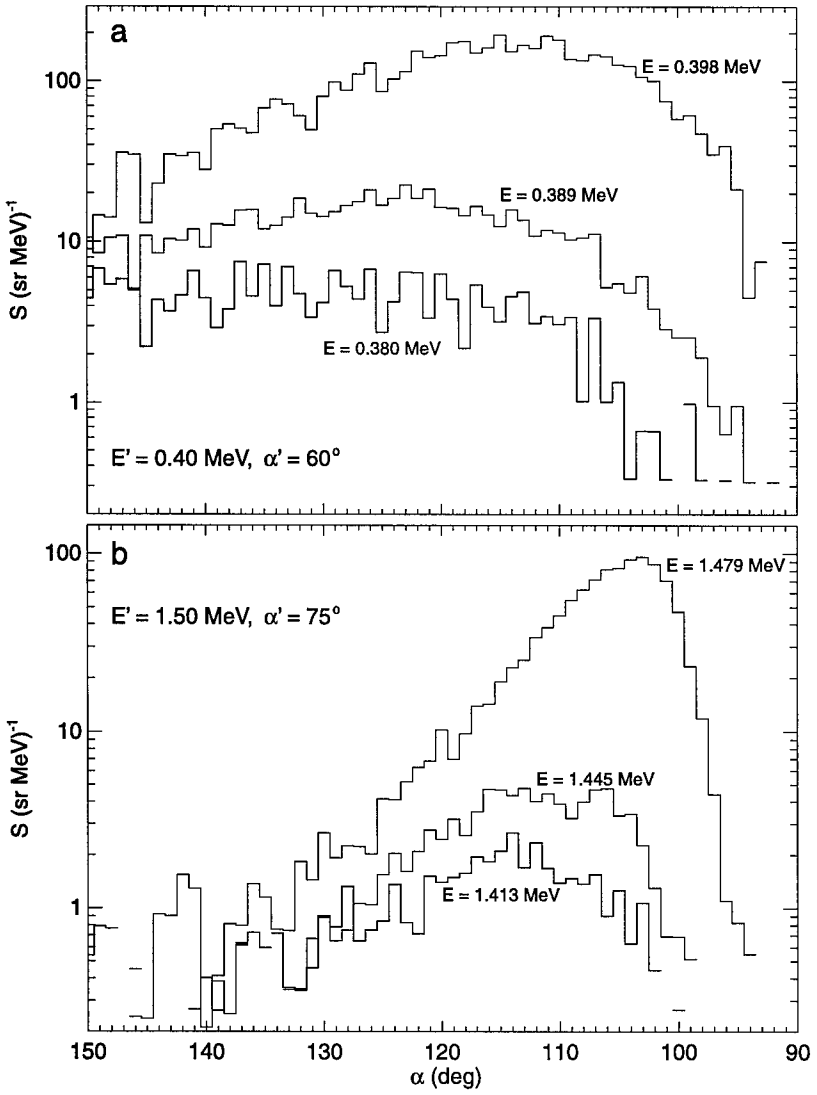

Figure 1. Backscattered electron pitch angle distributions at 205 km altitude from electrons entering the atmosphere with energy E' and pitch angle α' for three energies $E < E'$, calculated with the EGSnrc simulation.

loss rate, appropriately weighted by the spatial dependence of f.

[18] The distribution function f adjusts to changing conditions on three timescales: the diffusion timescale $\langle D_{xx} \rangle_b^{-1}$ $\sim$ days, the drift timescale $2\pi/\omega_d \sim$ minutes, and the bounce timescale $\tau_b \sim$ seconds. A numerical solution of the local transport equation (2) over all three timescales is impractical, because the time step must be a small fraction of the shortest timescale. Therefore the full numerical solution starts with the bounce and drift averaged equation (9) to obtain the x dependence of f on the diffusion timescale at x values outside the loss cones, proceeds to the bounce averaged equation (7) to obtain the x and ϕ dependences of f in and near the drift loss cone on the drift timescale, and finally returns to the local equation (2) to obtain the s, x and ϕ dependences of f in and near the bounce loss cones on the bounce timescale. At each stage the solution is followed until a steady exponential decay is reached after several intervals of the relevant timescale and the results of the first two stages become the initial condition for the next stage.

[19] The pitch angle diffusion operates in all three stages, but in the second and third stages it operates over smaller spatial scales determined by the extent of the drift and bounce loss cones that are filled by diffusion during a single drift and bounce period respectively, after which the electrons are lost. Therefore the drift and bounce timescales are sufficient to describe the diffusion during these stages.

[20] The main computational burden occurs in the final stage where the full solution in three dimensions (s, ϕ, and x) is obtained. The initial condition for this solution is improved by replacing the bounce averaged model with the backscattered distribution from each hemisphere inside the bounce loss cone for which the electrons are departing that hemisphere. This introduces the asymmetry about $x = 0$ that is caused by the differences between the north and south bounce loss cone angles and provides an initial condition that is fairly close to the final model.

[21] The numerical grid in s and x at a single grid point in ϕ, for the third stage of the numerical solution, is illustrated in Figure 4 (a finer grid is used in the actual calculation).

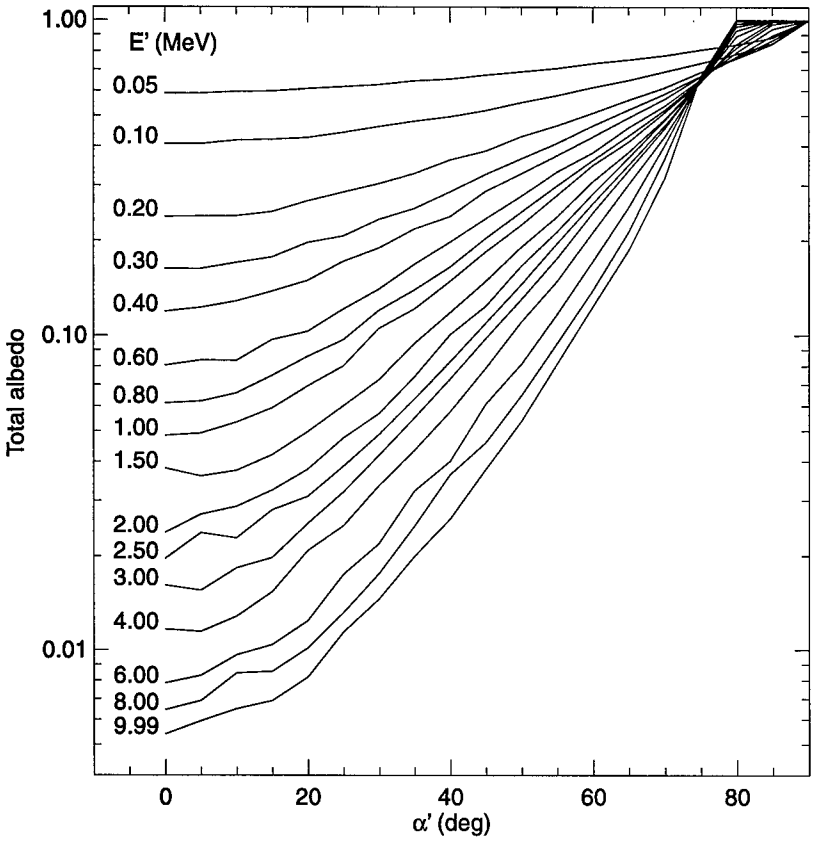

Figure 2. Calculated atmospheric electron total albedo, defined as the total number of backscattered electrons at any energy and pitch angle as a fraction of the number of incident electrons at a fixed energy E' and pitch angle α', versus α' for selected values of E'.

The grid spacing in s is determined by converting s to x_m, the x value for electrons mirroring at that s location, and then using the same grid spacing for x_m as for x [*Davidson and Walt*, 1977]. The scales in Figure 4 are nonlinear, with significantly finer spacing of grid points near the atmospheric boundaries in s and x because of the steeper gradients there. The direction of the bounce motion for a given x value determines the direction of the advective integration in s. When the integration reaches the atmosphere for x values inside either bounce loss cone then the backscattered distribution is calculated from (10) or (11) and this becomes the boundary condition for integration in s over the next half of the bounce motion. For x values outside both bounce loss cones, when a mirror point is reached then the current f value is used for the start of the next half of the bounce motion.

[22] The loss cone angles are calculated from the IGRF magnetic field model. However, the numerical grid along the field line is based on a dipole magnetic field. That is, the conversion from x_m back to s is based on the dipole formula for B/B_0, the ratio of local to equatorial magnetic field magnitudes. This is a good approximation for the inner magnetosphere, particularly given the weak dependence of the model solutions on s (see below). A dipole approximation is also used in calculating the azimuthal drift rate ω_d and the bounce period τ_b.

[23] The backscattered distribution at a given energy depends on the f values at higher energies. Therefore it is necessary to carry out the numerical solution over the whole range of energies simultaneously. The energy spectrum of the stably trapped population is imposed as an initial condition for each stage of the solution by a normalization factor at $x = 0$. The solution is sensitive to this choice of energy spectrum for x values within the loss cones.

3.2. Sample Electron Distributions

[24] Part of a sample numerical solution for $L = 3.5$ is shown in Figure 5. It includes the local pitch angle α and dipole longitude ϕ dependences of f at a fixed energy E and at a location s along the field lines for which $B/B_0 = 40$ (that would correspond to an altitude of 1430 km in a centered dipole approximation to the geomagnetic field). Figure 5 illustrates how the variation with ϕ in the size of the bounce loss cones causes the drift loss cone intensity to vary with longitude as a result of the balance between drift and pitch angle diffusion from the stable trapping region. Then, the resulting intensity in the drift loss cone at a given longitude determines the contents of the bounce loss cones at that longitude. The longitude ϕ is measured eastward in the dipole magnetic equator, starting from 0° geographic longitude, and increases in the same direction as the electron drift. Because this coordinate system rotates with the Earth and the magnetic local time dependence of the diffusion coefficient does not, it is necessary to perform the calculation at varying universal times, UT. In the case of Figure 5, UT = 0 and the noon maximum diffusion coefficient is at $\phi = 180°$.

[25] Model local pitch angle distributions at two fixed ϕ values are shown for selected energies in Figure 6. They

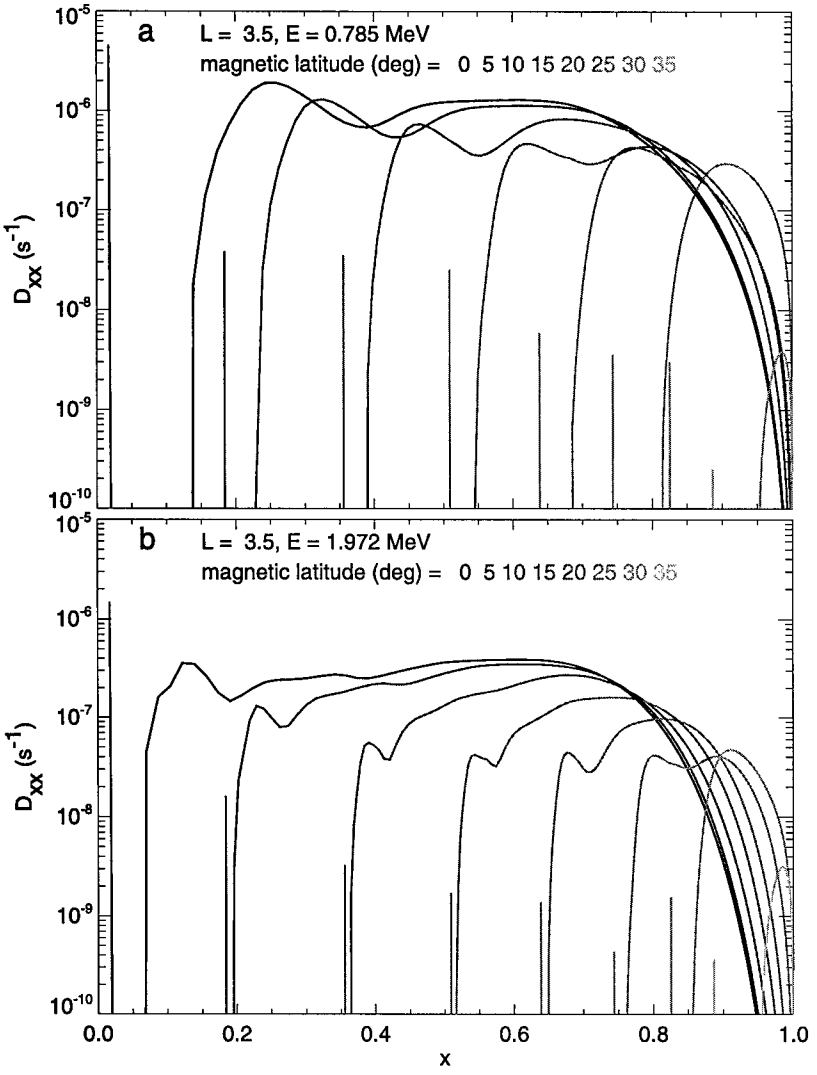

Figure 3. Diffusion coefficients versus $x = \cos \alpha_0$ for energy E and selected magnetic latitudes calculated from the plasmaspheric hiss whistler mode wave model described in the text. See color version of this figure in the HTML.

give a more detailed view of the bounce loss cone distributions over a range of energies. Electrons in the northern or southern bounce loss cone entering the atmosphere in the corresponding hemisphere are backscattered to form the bounce loss cone distributions entering the opposite hemisphere. Pitch angle diffusion during the bounce motion increases the intensity just inside the bounce loss cones sufficiently to maintain almost the same backscattered distribution on the next bounce. In the case of Figure 6a, for example, the southern bounce loss cone is larger than the northern one (because of the south Atlantic anomaly, or SAA) so that the electrons diffusing into the southern bounce loss cone come from the trapped population, whereas those diffusing into the northern bounce loss cone come from the lower southern bounce loss cone population. Therefore the backscattered intensity from the northern atmosphere in the northern bounce loss cone (at high pitch angles) is much lower than the backscattered intensity from the southern atmosphere in the northern bounce loss cone (at low pitch angles). These electrons are backscattered twice per bounce period whereas those outside the northern bounce loss cone but inside the southern bounce loss cone are backscattered once per bounce period, from the southern atmosphere only. The energy spectra in the bounce loss cones are considerably softer than those in the trapped distribution. This is a result of the generally lower albedo at higher energies (Figure 2). Also, the bounce loss cone spectra in Figure 6b are softer than those of Figure 6a because, at the longitude of Figure 6b, the drift loss cone intensities are reduced at the higher energies by the correspondingly higher drift rates.

[26] The sample solutions described above were specifically at the northern end of the field line. The solution is different at the southern end of the field line because of the diffusion into the bounce loss cones during a half bounce period. However, in these examples, the gradient $\partial f/\partial x$ is sufficiently steep near the bounce loss cone boundaries that the differences between the solutions at each end of the field line would not be apparent on the scale of the figures. Solutions at lower energies have a stronger dependence on s

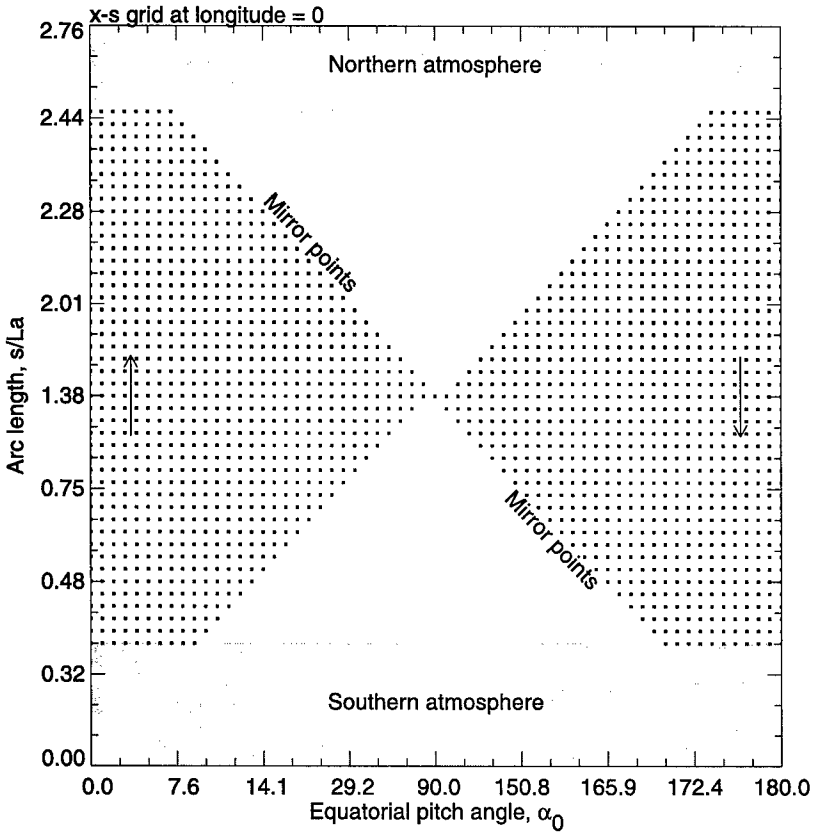

Figure 4. Subset of the numerical simulation grid at one longitude. The resolution is coarser than in the actual calculations. The arrows show the direction of the electron bounce motion for either side of α_0 = 90° (x = 0).

because of the longer bounce periods [*Davidson and Walt*, 1977].

[27] The model pitch angle distributions well inside the bounce loss cones at low and high pitch angles and at the higher energies show significant fluctuations (Figure 6). These are caused by the statistics of the Monte Carlo backscattering calculation (Figure 1) and do not adversely affect the final model simulations because they only occur where the backscattered intensities are low.

4. Data Comparisons

[28] We have selected three days for comparison of the model results with data taken by the PET instrument [*Cook et al.*, 1993; *Selesnick et al.*, 2003] on the low-altitude (~600 km), polar orbiting satellite SAMPEX. These days were chosen during periods of relatively steady electron decay following magnetic storm injections. They were also chosen as days with three differing average geomagnetic activity levels and for which there is little evidence of changes in the pitch angle diffusion rate during each day. The SAMPEX orbit crosses L = 3.5 ~60 times per day at varying longitudes and at two opposing local times. The data set from each day consists of the electron flux at each crossing from each of three electron counters labeled P1, ELO, and EHI, that measure electrons in the energy ranges of 0.6 MeV, ~1.5 to 6 MeV, and ~2.5 to 14 MeV, respectively. Each data point is at a given set of B/B_0, ϕ, and UT values, is in the northern or southern hemisphere, and covers a distinct range of x values corresponding to electrons with mirror points at and below the SAMPEX altitude. Equatorial pitch angles for mirror points at SAMPEX vary from ~7° to ~9.5°. Thus a particular model solution is used to simulate each data point by combining the model electron distribution function at each satellite location and UT of the measurement with the detailed instrumental energy and angular response functions for each electron counter (see *Selesnick et al.* [2003] for details of this method).

[29] The models for each day differ in their value of the noon maximum whistler wave field b_w and in the electron energy spectrum that normalizes the electron distribution at x = 0 (α_0 = 90°). All other model parameters are the same for each day. The normalizing energy spectra are from electron data taken at L = 3.5 by the HIST instrument [*Blake et al.*, 1995] on the high-altitude Polar satellite (see *Selesnick et al.* [2003] for examples of these spectra). In reference to both the Polar and SAMPEX data, L and B values were calculated with the IGRF magnetic field model.

[30] The data from SAMPEX and the model simulations of those data are shown in Figure 7a for 1997 day 186, Figure 7b for 1998 day 151, and Figure 7c for 1998 day 159. In each case, the observed and model fluxes for each rate counter are shown as a function of dipole longitude ϕ. Typically the highest fluxes are observed at southern longitudes from ~300° to ~30°E (the SAA region). These are stably trapped electrons, with mirror points that do not reach

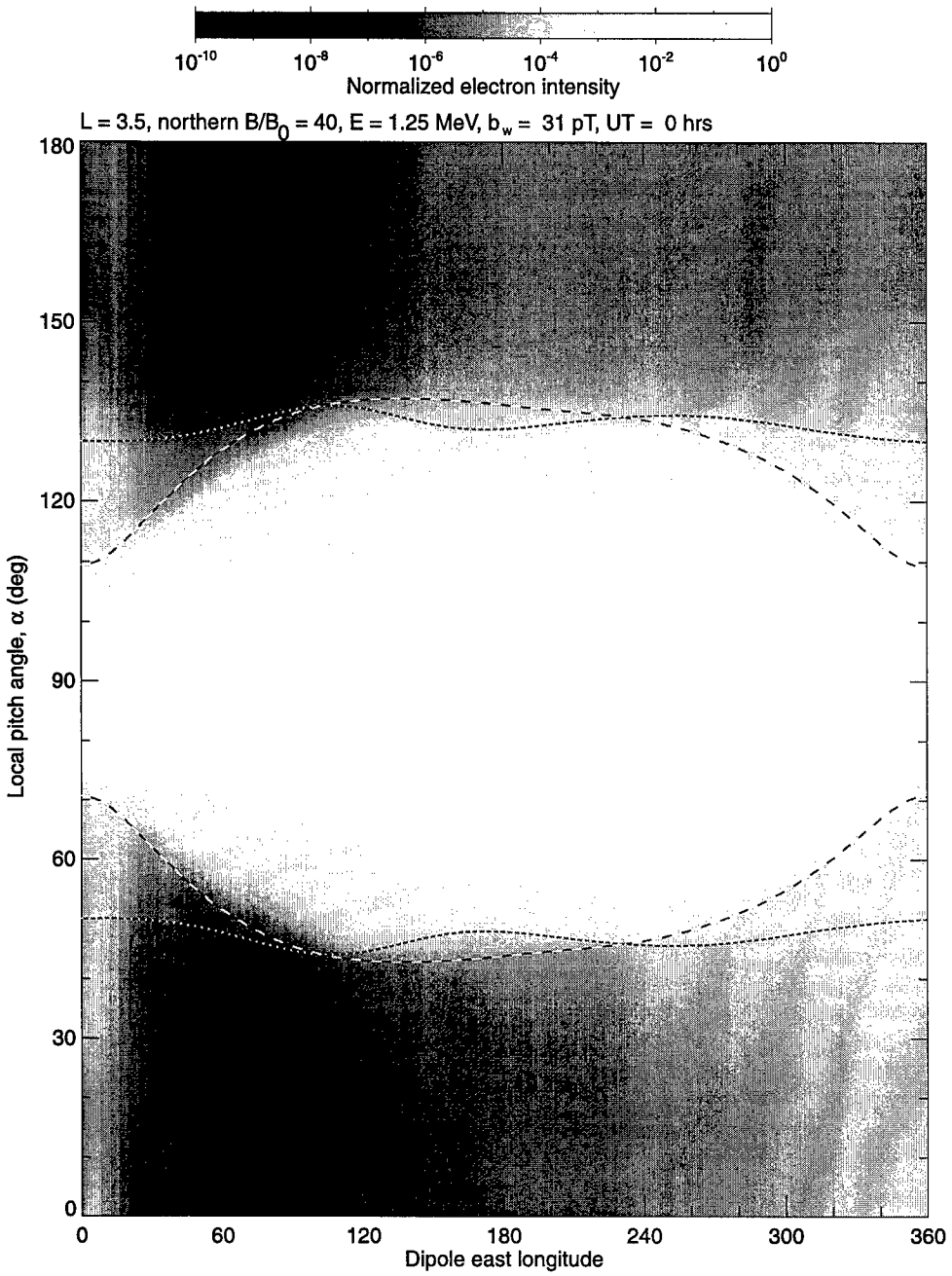

Figure 5. Sample simulated low-altitude electron distribution, showing the normalized electron intensity versus local pitch angle and dipole longitude for a fixed L shell, B/B_0, energy E, maximum wave magnetic field b_w, and universal time (UT). Dotted (dashed) curves indicate the north (south) bounce loss cone angles. See color version of this figure in the HTML.

the atmosphere at any longitude. The lowest fluxes are in a similar longitude range but from the northern hemisphere. These are untrapped electrons inside the bounce loss cone (BLC) that will enter the atmosphere within the next bounce. Their intensity is determined by the pitch angle diffusion rate into the bounce loss cones and by the atmospheric albedo. In the longitude range from ~30° to ~300°E, the fluxes generally are at intermediate levels and increase toward the east. These are the quasi-trapped electrons in the drift loss cone (DLC) that will reach the atmosphere within the next drift orbit. Their intensity is determined by the balance between the eastward drift and the pitch angle diffusion rate from the stably trapped population into the drift loss cone.

[31] The three sample days show similar characteristics in the variation of the electron intensity with geographic location of the data points. The main difference between them is in the relative intensity levels between the three regions, those of the stably trapped, quasi-trapped (drift loss cone) and untrapped (bounce loss cone) electrons. In the first case, 1997 day 186, the pitch angle diffusion rate was lowest, leading to less filling of the quasi-trapped and untrapped regions relative to the stable trapped region. In the third case, 1998 day 159, the pitch angle diffusion rate

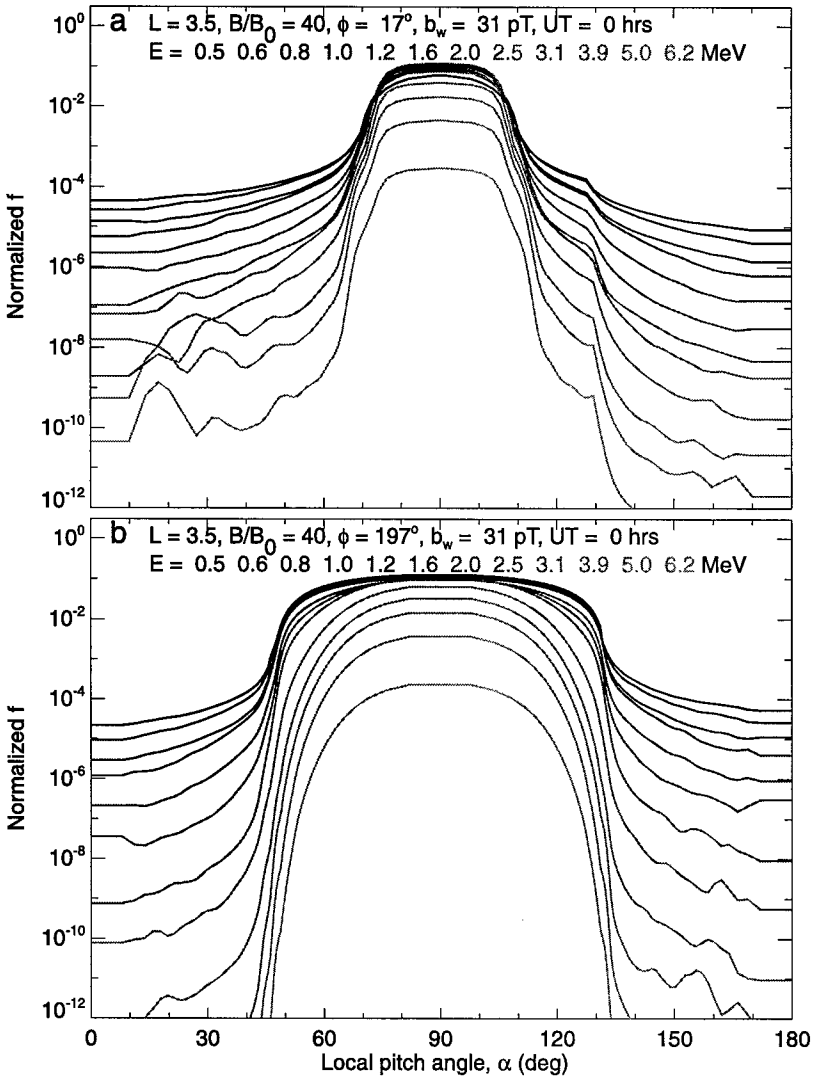

Figure 6. Simulated low-altitude pitch angle distributions from the same model solution as in Figure 5 but for two fixed dipole longitudes φ and selected electron energies *E*. See color version of this figure in the HTML.

was highest and so the quasi-trapped and untrapped regions contain relatively high electron intensities. The second case, 1998 day 151, was intermediate between the first and third. The absolute level of the stably trapped intensity also varies somewhat between the three cases as a result of the prior history of the radiation belt. This determines the dynamic range available to each rate counter above its rate of background counts (see *Selesnick et al.* [2003] for details).

[32] The average values of the D_{st} geomagnetic index during the low, medium, and high diffusion days were +1 (1997 day 186), −16 (1998 day 151), and −28 (1998 day 159), respectively, so they were all relatively quiet days, as is typical for periods of radiation belt decay following a geomagnetic storm. The correlation between the D_{st} index and the pitch angle diffusion rate (or electron lifetime) is described in more detail by *Selesnick et al.* [2003].

5. Discussion and Conclusion

[33] To model the geographic distribution of low-altitude radiation belt energetic electrons at a given L shell, it was necessary to include both the bounce and drift phase dependences in order to account for the longitude variations of the bounce and drift loss cone electron populations. The model included pitch angle diffusion at a rate derived from standard models of whistler mode waves in the plasmaspheric hiss frequency band and of the plasma density at L = 3.5. Three levels of wave magnetic field intensity were

Figure 7. Low-altitude satellite data and model simulations versus dipole longitude from the three electron rate counters (P1, ELO, and EHI) for three selected days. Each data point and its corresponding model simulation are connected by a dashed line. Model wave fields b_w correspond to (a) low, (b) medium, and (c) high pitch angle diffusion rates. See color version of this figure in the HTML.

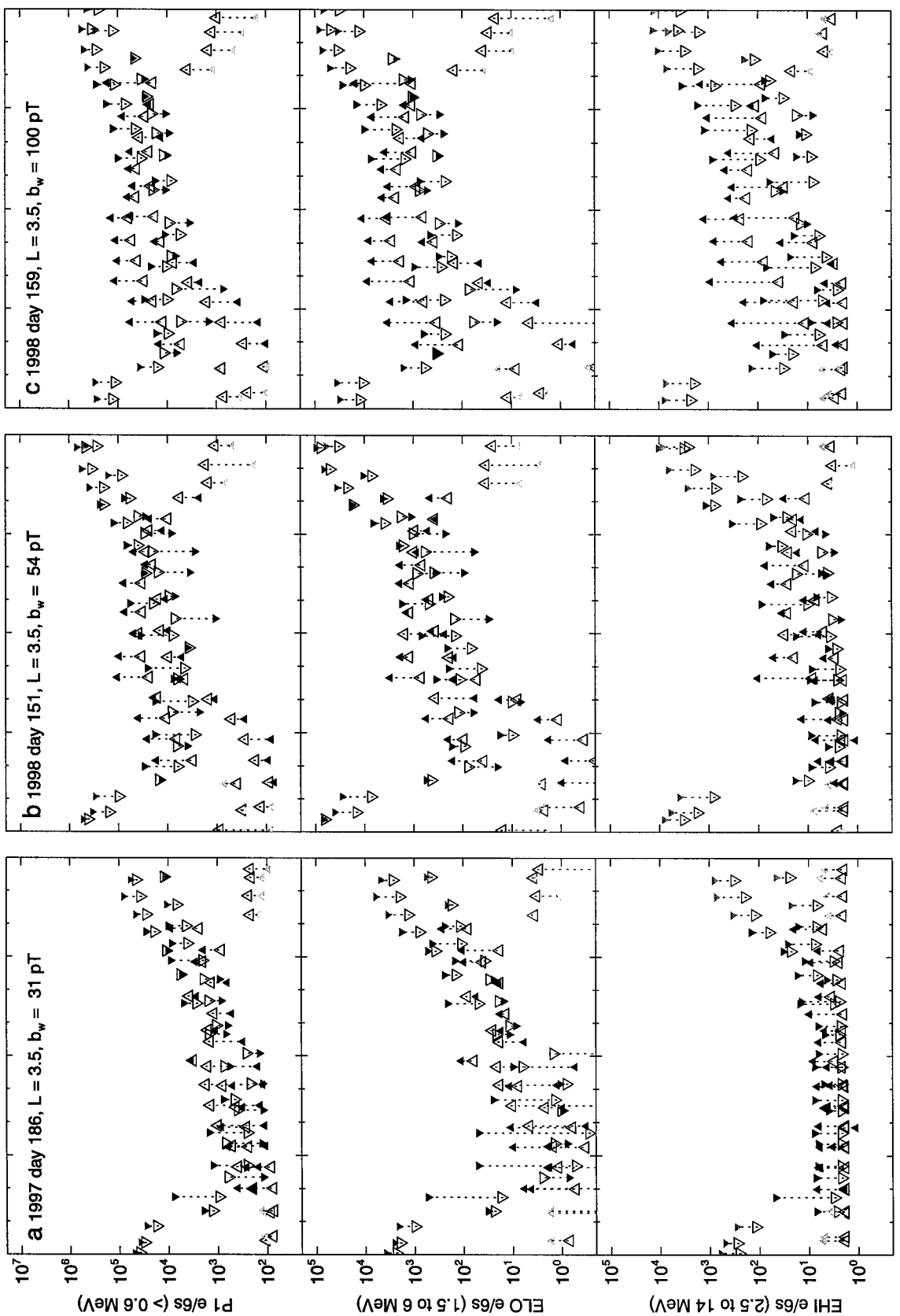
SAMPEX data: ▲▼North/south stably trapped ▲▼North/south quasi-trapped (DLC) △▽North/south untrapped (BLC) Simulation: △▽North/south
a 1997 day 186, L = 3.5, b_w = 31 pT
b 1998 day 151, L = 3.5, b_w = 54 pT
c 1998 day 159, L = 3.5, b_w = 100 pT
P1 e/6s (> 0.6 MeV)
ELO e/6s (1.5 to 6 MeV)
EHI e/6s (2.5 to 14 MeV)
Dipole longitude
0
90
180
270
360

Figure 7

chosen to normalize the diffusion rates for comparison of the model results with data taken on days with three correspondingly different geomagnetic activity levels. The model also included electron backscattering from a model atmosphere of realistic composition calculated with the EGSnrc Monte Carlo simulation.

[34] The model simulations and the SAMPEX electron data are in reasonable agreement for each of the three sample days (Figure 7), showing that the model includes the main factors that influence the low-altitude electron distribution during times of relatively steady radiation belt decay. While this is true for each day in an average sense, there are instances of fairly significant discrepancy between specific data points and their simulated values. There are several possible causes. First, the model parameters were not fit to the data. Only the wave magnetic field b_w was varied between the three cases and this was simply fixed at the three values judged to provide examples of low, medium, and high diffusion rates based on comparisons with the electron data. Second, the wave parameters including b_w and those affecting the wave spectrum and propagation directions are not well known even in an average sense. This is also true of the spatial distribution of the waves and of the plasma density in local time as well as along the magnetic field lines. Third, there can be changes in the diffusion rate during a day caused by varying wave and plasma conditions. While the sample days were chosen to minimize this possibility by comparison with data sets obtained on adjacent days, there must always be some temporal variability. Fourth, the backscattering calculation cannot be perfectly accurate, although, even with the various approximations involved, we expect that it should not be a major source of error because the inputs to the calculation are relatively well known. Fifth, the magnetic mapping between the high-altitude spectral measurements on Polar that are used to normalize the model and the low-altitude locations of SAMPEX may introduce some error. Sixth, the model neglects pitch angle diffusion by lightning and ground based VLF generated whistler waves and other wave modes. While these are significant at lower L values, their impact at $L = 3.5$ is thought to be minimal in a bounce and drift averaged sense [*Abel and Thorne*, 1998a]. However, it is possible that the lightning and VLF signals may make some significant contributions to the local pitch angle diffusion coefficient at certain times and longitudes related to the occurrences of thunderstorms and the geographic locations of VLF transmitters. These could be added to the model if the spatial and temporal distribution of the waves were known. Seventh and finally, the model does not include radial diffusion, energy diffusion, and possibly other radiation belt processes that may be of some significance.

[35] While there is a long list of possible improvements, it is likely that the greatest source of error is in the plasmaspheric hiss wave model that determines the pitch angle diffusion rate. Some evidence of this can be seen in the comparisons with the SAMPEX data. First, the higher energy electron measurements (the EHI data) tend to disagree with the simulations to a greater extent than those at lower energies. This may be indicative of an inaccuracy in the energy dependence of the calculated diffusion coefficients. Second, the normalization of the model by the high-altitude Polar data does not always lead to an accurate prediction of the overall stably trapped intensity level observed on SAMPEX. This can be a result of inaccurate distribution of wave power along the magnetic field. For example, a reduction in the relative wave intensity at high magnetic latitudes would reduce the equatorial pitch angle dependence of the electron intensity in the stable trapping region and increase the simulated low-altitude stably trapped intensity. These considerations show that improved measurements of the spatial, temporal, and frequency distribution of whistler and possibly other wave modes could allow more accurate modeling of the low-altitude radiation belt electron distribution.

[36] **Acknowledgments.** This work was supported by NASA under grant NAG5-12766 and by the Space Vehicles Directorate of the Air Force Research Laboratory.

[37] Arthur Richmond thanks Rumi Nakamura for her assistance in evaluating this paper.

References

Abel, B., and R. M. Thorne (1998a), Electron scattering loss in the Earth's inner magnetosphere: 1. Dominant physical processes, *J. Geophys. Res.*, *103*, 2385.

Abel, B., and R. M. Thorne (1998b), Electron scattering loss in the Earth's inner magnetosphere: 2. Sensitivity to model parameters, *J. Geophys. Res.*, *103*, 2397.

Albert, J. M. (1999), Analysis of quasi-linear diffusion coefficients, *J. Geophys. Res.*, *104*, 2429.

André, R., F. Lefeuvre, F. Simonet, and U. S. Inan (2002), A first approach to model the low frequency wave activity in the plasmasphere, *Ann. Geophys.*, *20*, 981.

Blake, J. B., et al. (1995), CEPPAD: Comprehensive energetic particle and pitch angle distribution experiment on POLAR, *Space Sci. Rev.*, *71*, 531.

Cook, W. R., et al. (1993), PET: A proton/electron telescope for studies of magnetospheric, solar, and galactic particles, *IEEE Trans. Geosci. Remote Sens.*, *31*, 557.

Davidson, G., and M. Walt (1977), Loss cone distribution of radiation belt electrons, *J. Geophys. Res.*, *82*, 48.

Kawrakow, I., and D. W. O. Rogers (2000), The EGSnrc code system: Monte Carlo simulation of electron and photon transport, *Tech. Rep. PIRS-701*, Natl. Res. Counc. of Can., Ottawa, available at http://www.sao.nrc.ca/inms/irs/EGSnrc/pirs701/index.html.

Lyons, L. R. (1974), Pitch angle and energy diffusion coefficients from resonant interactions with ion-cyclotron and whistler waves, *J. Plasma Phys.*, *12*, 417.

Picone, J. M., A. E. Hedin, D. P. Drob, and A. C. Aikin (2002), NRLMSISE-00 empirical model of the atmosphere: Statistical comparisons and scientific issues, *J. Geophys. Res.*, *107*(A12), 1468, doi:10.1029/2002JA009430.

Retterer, J. M., J. R. Jasperse, and T. S. Chang (1983), A new approach to pitch angle scattering in the magnetosphere, *J. Geophys. Res.*, *88*, 201.

Selesnick, R. S., J. B. Blake, and R. A. Mewaldt (2003), Atmospheric losses of radiation belt electrons, *J. Geophys. Res.*, *108*(A12), 1468, doi:10.1029/2003JA010160.

Smith, E. J., A. M. A. Frandsen, B. T. Tsurutani, R. M. Thorne, and K. W. Chan (1974), Plasmaspheric hiss intensity variations during magnetic storms, *J. Geophys. Res.*, *79*, 2507.

Walt, M. (1966), Loss rates of trapped electrons by atmospheric collisions, in *Radiation Trapped in the Earth's Magnetic Field*, edited by B. M. McCormac, p. 37, D. Reidel, Norwell, Mass.

J. M. Albert, Air Force Research Laboratory/VSBX, 29 Randolph Rd., Hanscom AFB, MA 01731-3010, USA.

M. D. Looper, The Aerospace Corporation, P.O. Box 92957-M2/260, Los Angeles, CA 90009-2957, USA.

R. S. Selesnick, The Aerospace Corporation, P.O. Box 92957-M2/259, Los Angeles, CA 90009-2957, USA. (richard.s.selesnick@aero.org)